Hindawi
Geofluids
Volume 2023, Article ID 7223392, 15 pages
https://doi.org/10.1155/2023/7223392

Research Article

Multidimensional Analysis of Precursor Information of Rockburst during Loading and Unloading of Deep Diorite

Jian Liu and Zonghong Zhou

School of Land and Resources Engineering, Kunming University of Science and Technology, Kunming, Yunnan 650000, China

Correspondence should be addressed to Zonghong Zhou; zhou20051001@163.com

Received 25 January 2023; Revised 6 March 2023; Accepted 7 March 2023; Published 19 May 2023

Academic Editor: Constantinos Loupasakis

At present, rockburst disasters cannot be predicted accurately, and the prevention and control of deep underground engineering disasters are significantly challenging. To explore the evolution law of precursory information of rockburst instability, the rockburst test of diorite was conducted with high confining pressure and different unloading rates (0.1 MPa/s, 0.3 MPa/s, 0.5 MPa/s, 0.7 MPa/s, and 0.9 MPa/s). Multidimensional analysis is carried out by evaluating deformation features, fast Fourier transform (FFT), energy entropy, singular spectrum entropy, and power spectrum entropy. The results show that Poisson's ratio is hook-shaped before rockburst, the elastic modulus is in the shape of a step, ringing count and energy surge after a quiet period, three-dimensional law of $0.98\sigma_c \sim \sigma_c$ stress location space shows a large red ball distribution along the shear plane, b value fluctuates in the low-value range, and low-frequency high amplitude and high-frequency low amplitude fluctuate in a large range after 300 s, with frequent abnormal fluctuations of the energy spectrum entropy, the singular spectrum entropy, and the power spectrum entropy curve. The above research results can be considered the evolution law of rockburst precursor information, which enriches the theoretical method of explosion disaster prediction.

1. Introduction

Rockburst, one of the research hotspots in the fields of rock engineering, mining engineering and water conservancy, and hydropower engineering, directly threatens the safety of practical engineering. Generally, the rock mass on the excavation side is likely to generate rockburst disasters when the accumulated strain energy inside the rock mass is sufficiently large. However, rockburst cannot be accurately predicted due to the characteristics of emergencies, nonlinearity, and destructiveness, which are very adverse to the safety of practical engineering [1–4].

In recent years, most researchers have studied rockburst disasters, mainly focusing on mechanism analysis [5–7], laboratory tests [8–11], numerical simulation [12–17], field monitoring [18–22], and rockburst prediction [23–26]. He et al. [27] developed a set of rockburst test devices that divide rockbursts into impact types and induced types and use an energy-absorbing anchor to control rockburst disasters. Ren et al. [28] carried out acoustic emission tests on porous siltstone specimens, studied the shape of the failure zone around the hole, and combined the fractal dimension of the nuclear density function with the butterfly profile to predict the occurrence time of rockburst. Keneti and Sainsbury [29] studied a large number of rockburst cases and identified the conditions leading to rockburst, which provided a basis for the prediction of rockburst utilizing numerical simulation. Ma et al. [30] carried out real-time monitoring of rockburst disasters through microseismic monitoring and proposed some criteria, such as stress spatial evolution, magnitude, and energy concentration of microseismic events and abrupt change of apparent volume. Dong et al. [31] selected uniaxial compressive strength, uniaxial tensile strength, elastic performance index, and other parameters as indicators and used random forest, SVM, and an artificial neural network to predict rockburst grade.

However, the analysis of rockburst mechanisms and on-site monitoring theory is not sufficiently deep; there is a gap between numerical simulation modeling and actual rockburst engineering, and there are few actual engineering

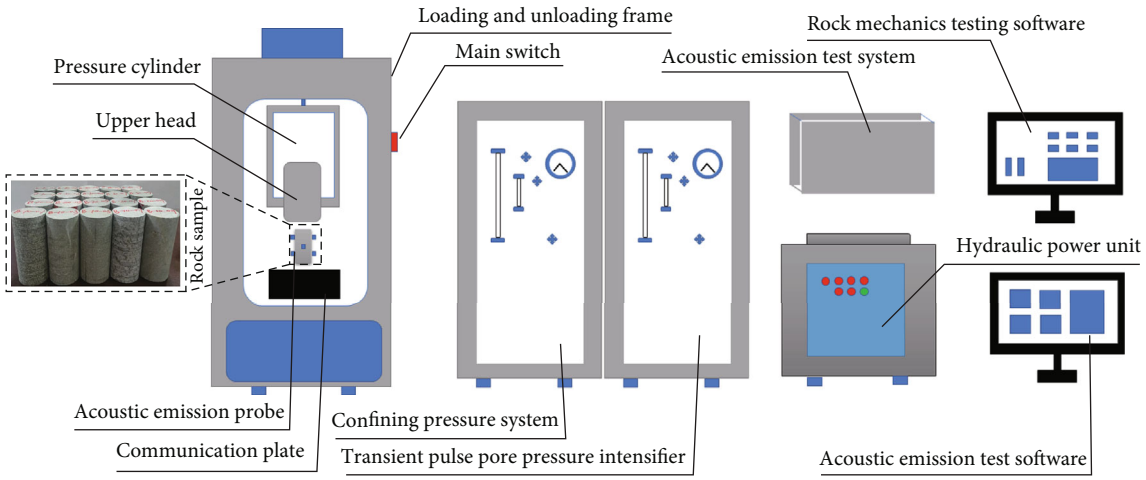

Figure 1: Rock mechanics test system.

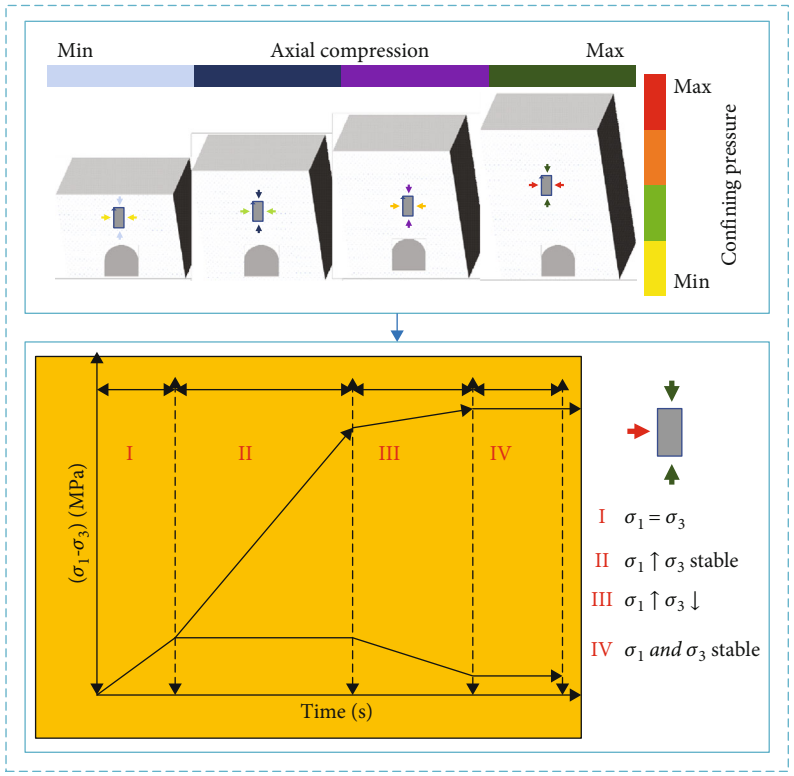

Figure 2: Loading diagram of the triaxial unloading test.

indicators in rockburst prediction. Accurate rockburst early warning cannot be achieved. The key problem of rockburst early warning is the identification of failure characteristic information in the process of rockburst gestation. In this paper, according to the rockburst disaster mechanism induced by stress disturbance, an unloading test of increasing axial pressure and unloading confining pressure is designed, and a variety of methods are adopted to cooperatively capture the evolution law of rockburst failure characteristic precursory information.

At present, the main research results of rockburst precursory information are as follows: Lu et al. [32] carried out experimental research and theoretical analysis on the F_{16} fault rockburst in the 25110 working faces, excavated rockburst precursory information, and proposed blasting and drilling pressure relief to control rockburst disasters. Wang et al. [33] carried out a field investigation of rockburst, analyzed the influence of structure on rockburst, studied the temporal and spatial distribution map and energy density map of microseismic data, and revealed the precursory

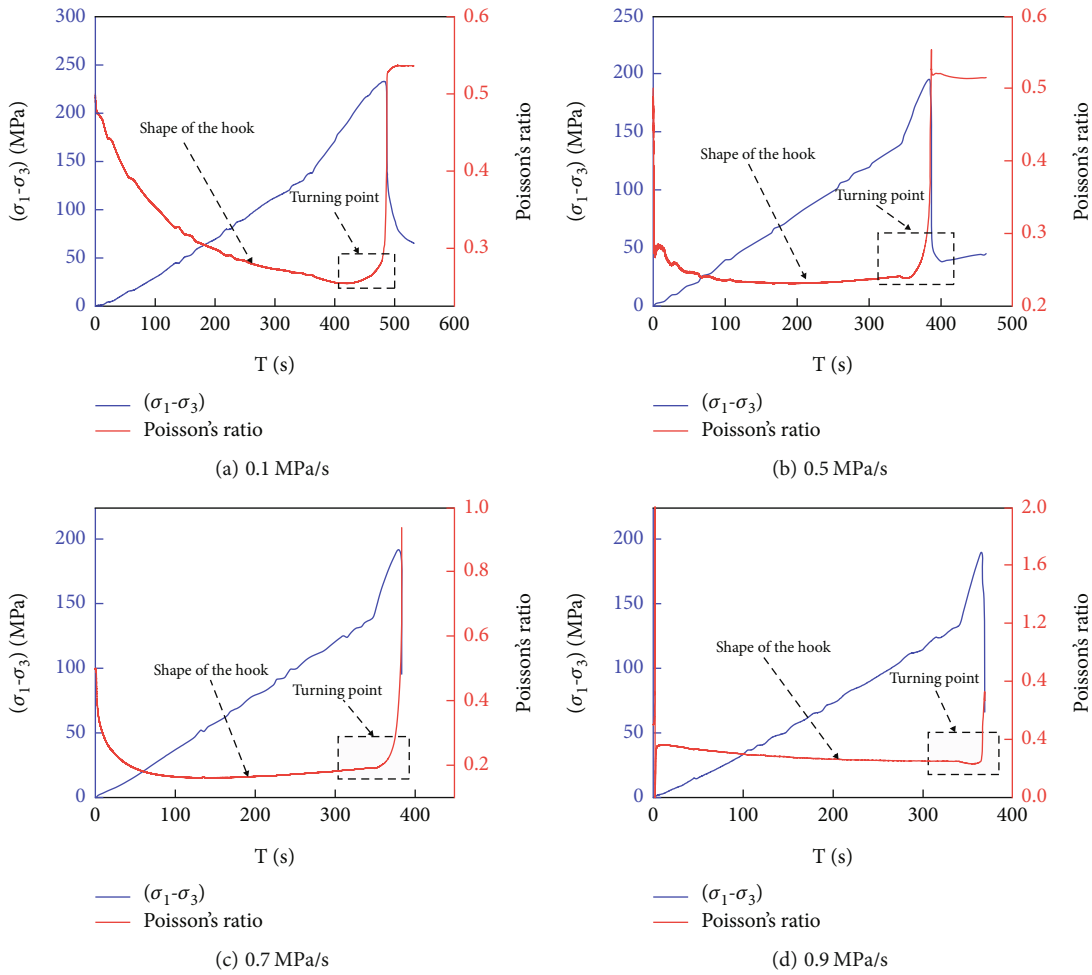

Figure 3: Variation in Poisson's ratio at different unloading rates of 40 MPa confining pressure.

information of rockburst. Liu et al. [34] studied the influence of water content on rockburst disasters. The acoustic emission parameter event rate and acoustic emission energy rate were analyzed by using an acoustic emission (AE) monitoring system and an infrared thermal imager. Ding et al. [35] carried out unloading experiments on limestone and analyzed indices such as acoustic emission energy, damage analysis, and RA. Liang et al. [36] carried out a triaxial test and analyzed the variation law of amplitude, b value, and temperature in the process of roadway deformation. Gong et al. [37] analyzed the frequency spectrum of acoustic emission signals and found that there was a frequency shift in the process of rockburst. Wang and Lin et al. [38, 39] carried out rockburst experiments to analyze acoustic emission data and reveal precursory characteristics through the characteristics of parameters and frequency spectra. He et al. [40] carried out joint monitoring tests of acoustic emission and electromagnetic radiation for coal and rock specimens and revealed the precursory information of rockburst through the analysis of energy and damage. Zhai et al. [41] carried out experiments on granite using a high-speed camera and acoustic emission to monitor and capture the precursory information of rock fractures. Xue et al. [42] used microseismic monitoring to analyze the main frequency of stress and reveal the precursory information of the rockburst process. According to previous studies, acoustic emission parameter event rate, energy rate, damage analysis, RA, and infrared radiation energy analysis have been studied extensively, and the frequency spectrum analysis of acoustic emission waveform data is mostly time-frequency analysis and amplitude-frequency analysis. At present, the above research cannot realize the identification of rockburst precursory information, and it is necessary to continually enrich the theoretical methods used for this purpose.

In this paper, according to the actual situation of Yuanyang Daping Gold Mine and the induced mechanism of rockburst, the test of unloading confining pressure is carried out to simulate the sudden failure process of rockburst. The failure process of rock is accompanied by a large number of acoustic emission phenomena, and the acoustic emission signal can reflect the process of rock failure [43–45]. The AE signals collected are analyzed for deformation characteristics, ring count, energy, b value, energy entropy, singular spectrum entropy, and power spectrum entropy, and multidimensional analysis is carried out to elucidate the evolution law of precursory rockburst information to enrich the cooperative early warning theory of rockburst disasters.

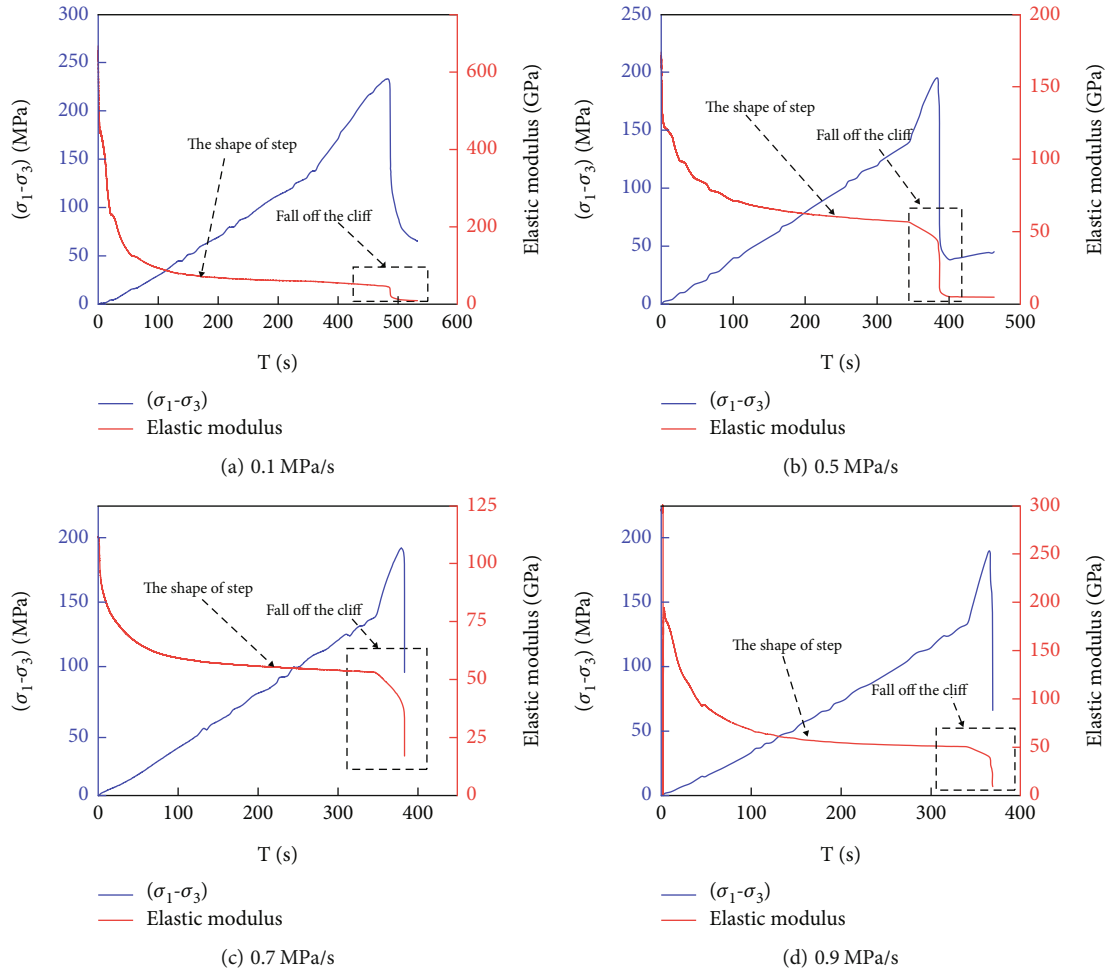

Figure 4: Variation in the elastic modulus at different unloading rates of 40 MPa confining pressure.

2. Test Equipment and Scheme

2.1. Equipment. The test adopts the American GCTS RTX-3000 rock testing system, which includes a loading system, measuring system, and console. The test standard conforms to the American ASTM D2664-04 and ISRM standards. The acoustic emission adopts the acoustic emission system of American Physical Acoustics Company, and six probes are used for data acquisition in this experiment. The threshold value of the acoustic emission parameter 40 dB is used to reduce the influence of the surrounding noise on the test, and the sampling distance parameter sampling frequency of 1 MHz is set. The rock samples are taken from the levels of 510 m and 560 m in the middle section of the Daping gold deposit, Yuanyang, Yunnan Province. The main rocks are diorite, and some rock samples are prepared as shown in Figure 1.

Step 1. Start the GCTS RTX-3000 test system, acoustic emission test system, hydraulic power unit, and air compressor. The screened samples are loaded into the prepared heat-shrinkable pipe, steel blocks of the same size are fixed at both ends of the heat-shrinkable pipe, and the rock samples are fixed together with the upper and lower steel blocks.

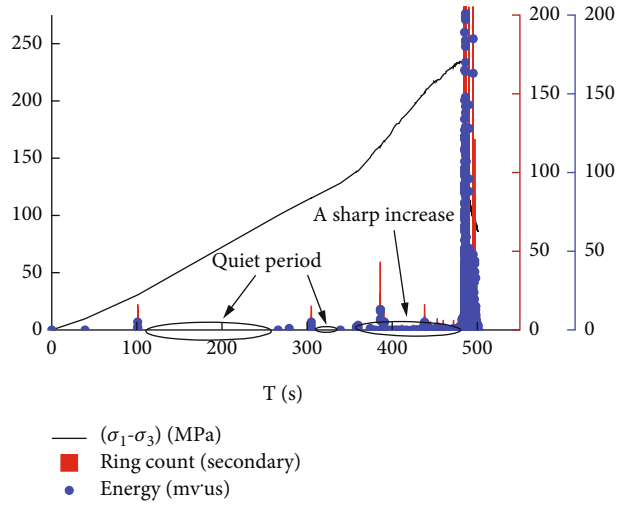

Figure 5: Diorite stress-ringing count (energy)—time curve for an unloading rate of 0.1 MPa/s.

Step 2. The hot air gun is used to heat the rock sample and moves slowly to both sides in the middle. When the sample, the upper and lower steel blocks, and the heat shrinkable

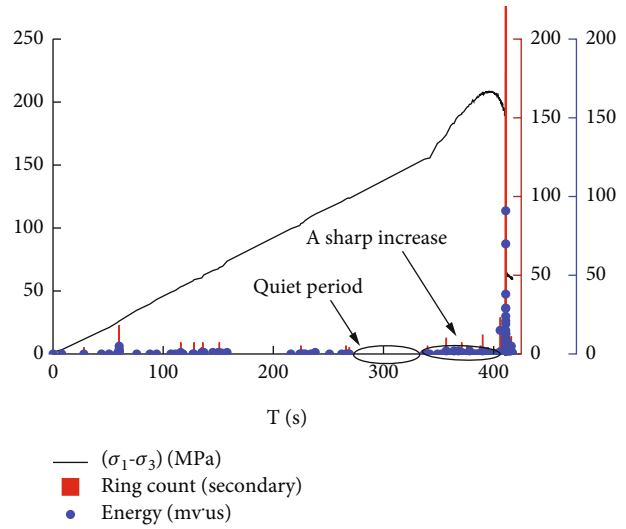

FIGURE 6: Diorite stress-ringing count (energy)—time curve for an unloading rate of 0.3 MPa/s.

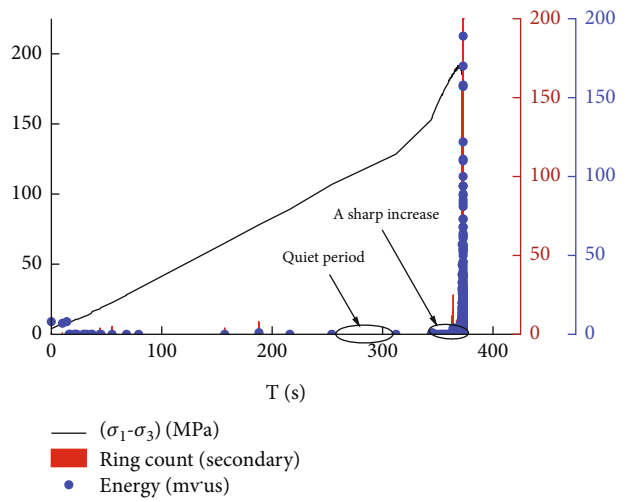

FIGURE 7: Diorite stress-ringing count (energy)—time curve for an unloading rate of 0.5 MPa/s.

pipe are fully fitted, close the hot air gun and check whether the upper and lower steel blocks are completely coincident with the sample on the midline.

Step 3. Install the axial displacement meter and the radial extension meter and connect the communication plate of the bottom seat. Adjust the upper and lower rings until they are concentric, so that the two guide rods move freely. The acoustic emission positioning probe is arranged, the acoustic emission probe is connected to the bottom plate communication seat, and the probe coated with special glue is fixed with a rubber band.

Step 4. The extensometer and acoustic emission probe tests are carried out, and the axial extensometer nut knob test range is manually adjusted. Adjust the measuring range of the nut knob of the radial extensometer to avoid the over-range phenomenon in the test process. The collective effect of the acoustic emission probe is tested, and the elastic wave received by each probe is tested by tapping on the top of the sample. After completing the test, push the base of the sample into the lower part of the pressure cylinder.

Step 5. Apply pressure to prestress the sample and use displacement control to slowly lower the upper pressure head until the sample makes contact to remove the displacement; instead of stress control, apply the initial force of 2 kN to ensure the complete contact of the sample.

Step 6. The pressure cylinder is slowly put down to ensure that the cylinder wall is not in contact with the communication line, the confining pressure test system injects oil into the pressure cylinder, and the computer program is used to set up the loading and unloading program to start the test.

2.2. Test Scheme. To more accurately simulate the rockburst process of deep mining in the Yuanyang Gold Mine, a reasonable in situ stress must be determined. The Yuanyang

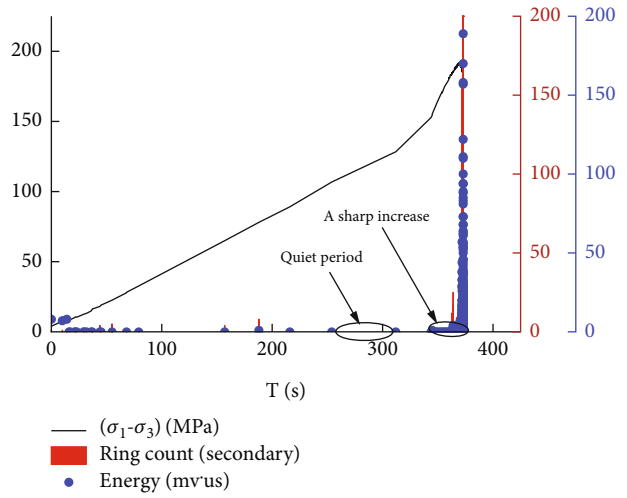

FIGURE 8: Diorite stress-ringing count (energy)—time curve for an unloading rate of 0.7 MPa/s.

Gold Mine does not carry out actual in situ stress measurements. By consulting the relevant literature and comparing similar mines, a reasonable stress level is determined. Referring to the actual situation of similar mines, combined with the current mining depth of approximately 800 m in the Yuanyang Gold Mine, and considering that it is about to enter deeper mining, the maximum horizontal stress is set to 40 MPa [46, 47].

Step 1. The confining pressure test of axial compression unloading was used to simulate the process of rockburst. The test is divided into four stages: the loading system sets the initial pressure difference to 2 ~ 3 kN.

Step 2. Increase the confining pressure and apply the confining pressure to predetermined values of 10 MPa, 20 MPa,

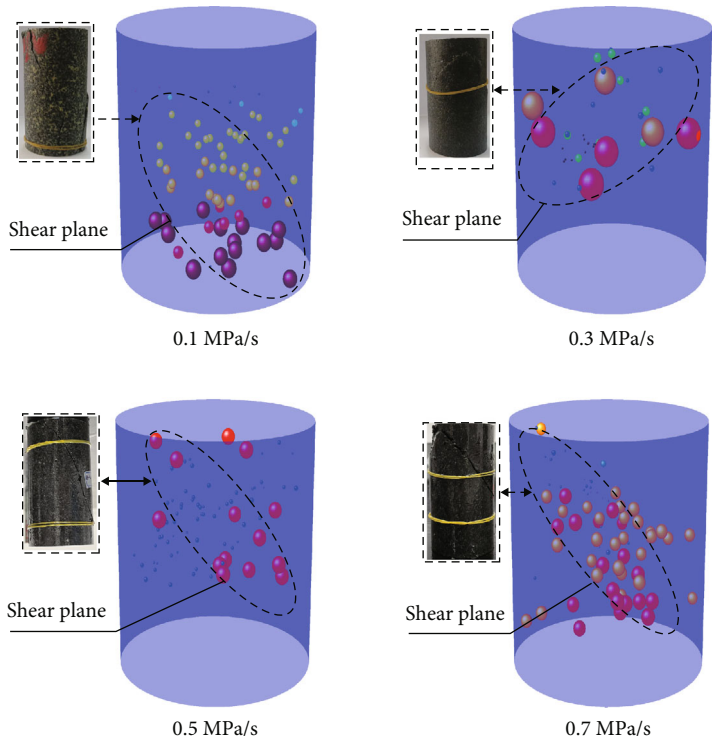

Figure 9: Spatial evolution diagram of stress location under different unloading rates of 40 MPa confining pressure.

30 MPa, and 40 MPa (the rates are approximately 6 MPa/min and 0.1 MPa/s).

Step 3. Use the displacement control method to increase σ_1 to a certain stress state (before the peak) under the condition that σ_3 is constant. The confining pressure is unloaded at a certain rate (0.1 MPa/s, 0.3 MPa/s, 0.5 MPa/s, 0.7 MPa/s, and 0.9 MPa/s) with increasing axial pressure.

Step 4. The test sets three unloading rates: fast, medium, and slow. In the test of the postfailure effect of the specimen, once the specimen is destroyed, it stops reducing the confining pressure and keeps it unchanged; at the same time, the axial stress continues to be applied until the stress difference $(\sigma_1\text{-}\sigma_3)$ does not decrease with increasing axial strain, as shown in Figure 2.

3. Analysis of the Test Results

3.1. Deformation Feature Analysis

3.1.1. Analysis of the Evolution of Poisson's Ratio. The change law of Poisson's ratio with different unloading rates at the same confining pressure is studied. Due to the limited space, Yuanyang Gold Mine is about to enter the stage of deep mining. This section only studies the variation in Poisson's ratio at a confining pressure of 40 MPa, as shown in Figure 3.

Under the condition of increasing axial compression and unloading confining pressure, the variation in Poisson's ratio of diorite can be divided into four stages. At the initial stage of loading, the Poisson's ratio of diorite is larger. With the continuous increase in load, the Poisson's ratio of diorite begins to decrease sharply. With the further increase in load, a relatively low level of Poisson's ratio appears in diorite before rockburst. When rockburst occurs, the Poisson's ratio of diorite increases step by step, and Poisson's ratio shows the opposite configuration as a whole. As shown in Figure 3(a), Poisson's ratio was 0.25 at 437 s and reached the peak intensity at 482 s, with Poisson's ratio rising rapidly. In Figure 3(b), Poisson's ratio was 0.23 at 348 s and reached the peak intensity at 383 s, with Poisson's ratio rising rapidly; in Figure 3(c), Poisson's ratio was 0.19 at 351 s and reached the peak intensity at 373 s, with Poisson's ratio rising rapidly; in Figure 3(d), Poisson's ratio was 0.23 at 355 s and reached the peak intensity at 364 s, with Poisson's ratio rising rapidly; Poisson's ratio is an important index reflecting the mechanical properties of rock, which can reflect the process of crack initiation, propagation, nucleation, overall strength decline, and overall instability of rock. When a rockburst occurs, deformation and radial sharp strain increase, and Poisson's ratio increases accordingly.

3.1.2. Analysis of the Evolution of Elastic Modulus. This section studies the change law of the elastic modulus of the same confining pressure and different unloading rates, and this section only studies the change law of the 40 MPa elastic modulus of confining pressure as shown in Figure 4.

The deformation modulus of diorite under increasing axial compression and unloading confining pressure can be roughly divided into three stages. At the initial stage of loading, the deformation degree of the rock sample is relatively small, and the deformation modulus of the rock sample is

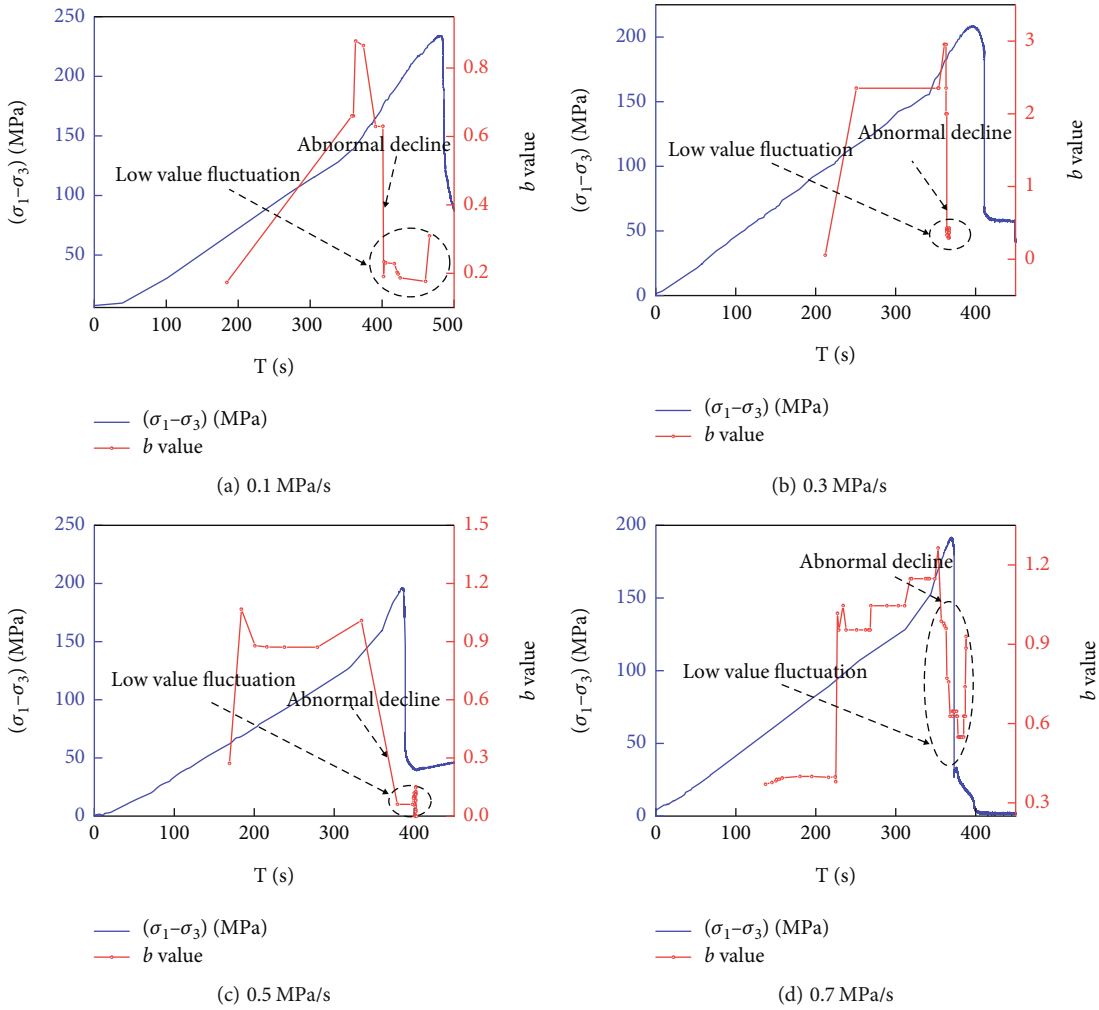

Figure 10: Analysis of the b value with different unloading rates for the same confining pressure.

larger. With the continuous increase in load, the rock sample has a large deformation; the deformation modulus falls sharply and then remains stable. Immediately prior to the rockburst, the rock sample has a large deformation again, and the deformation modulus falls sharply again. The elastic modulus is generally step like, and the deformation modulus is an index reflecting the deformation degree of rock samples.

3.2. Stress-Ring Count (Energy): Time Evolution Law. The ringing count and energy analysis of acoustic emission data can reflect the catastrophic process of rockburst, as shown in Figures 5–8. The curve of the stress-ring count (energy)—time with different unloading rates with the same confining pressure, is described. At the initial stage of the confining pressure test, the ring count and energy occasionally appear with increasing stress. With the continuous increase in load, there is a relatively quiet period between ring count and energy (100.3 s to 256.5 s in 0.1 MPa/s, 270.6 s to 322.3 s in 0.3 MPa/s, 242.5 s to 314.8 s in 0.5 MPa/s, and 250.7 s to 308.3 s in 0.7 MPa/s). With a further increase in load, the ring count and energy increased sharply immediately before the rockburst disaster (477.1 s to 486.8 s at 0.1 MPa/s, 330.8 s to 408.1 s at 0.3 MPa/s, 358.3 s to 387.5 s at 0.5 MPa/s, and 341.6 s to 363.4 s at 0.7 MPa/s). The catastrophic process of rockburst exhibits a quiet period and explosive growth stage, and the quiet period and surge of ring count (energy) can be taken as precursory rockburst information.

3.3. Study on the Three-Dimensional Evolution Law of Stress-Location Space. In this paper, the AE software positioning data are exported to a txt file, and the location coordinates and time of AE signals are obtained. After the AE positioning information is processed by MATLAB software, the spatial evolution characteristic map of AE positioning information is drawn.

As shown in Figure 9, according to the relationship between the three-dimensional coordinates and stress of acoustic emission positioning events, a three-dimensional evolution diagram of the acoustic emission stress positioning space is drawn. The size of the balls maps the stress from small to large, and their colors indicate the volume size positioning (black: small volume positioning; blue: medium and small volume positioning; green: medium volume positioning; orange: medium and large volume positioning; and red: large volume positioning). The catastrophic process of

Table 1: Change rate of the b value at the same unloading rate.

Unloading rate (MPa/s)	0.1	0.3	0.5	0.7
Maximum decreasing rate of b value	0.69	0.87	0.94	0.51
T/s	402	363	(335, 378)	352

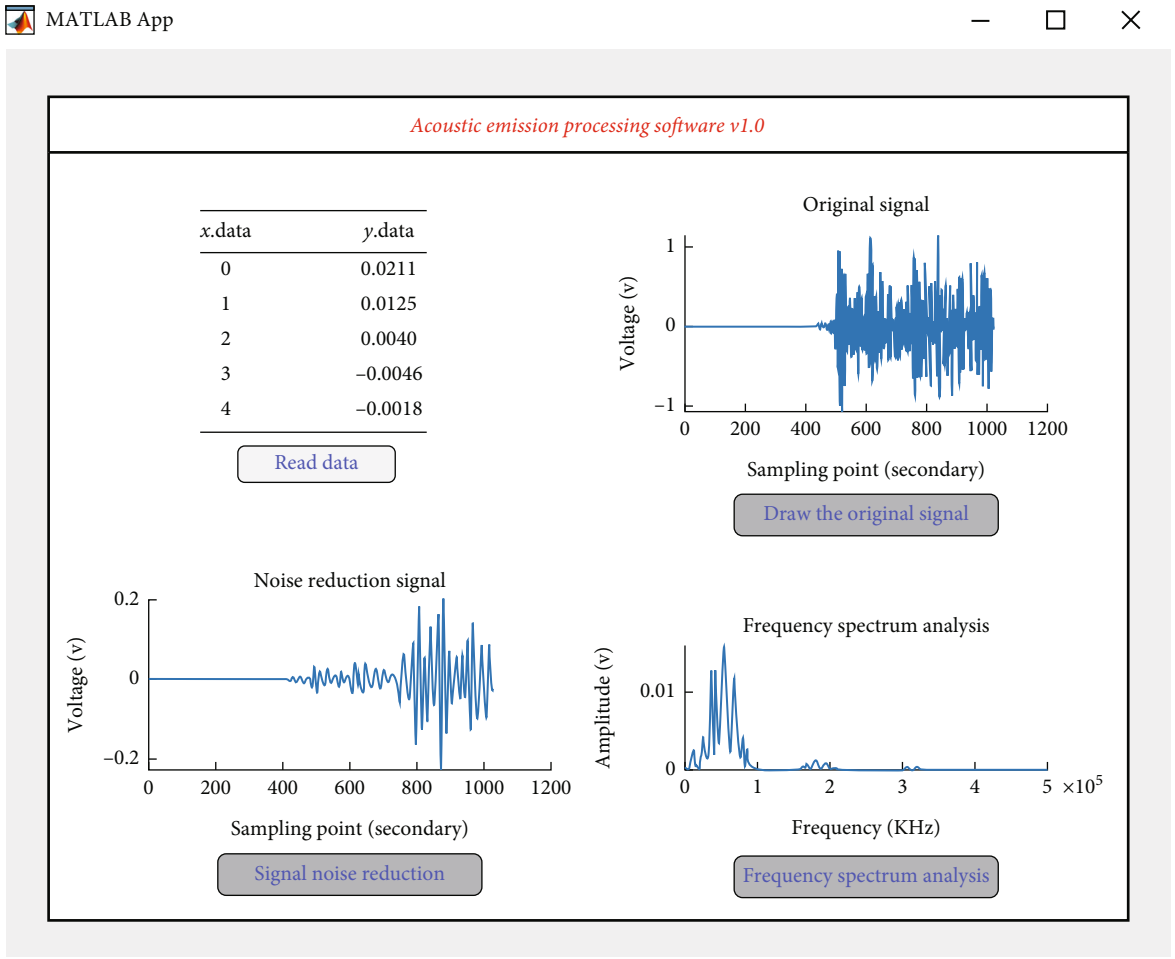

Figure 11: Acoustic emission processing software.

the rockburst is revealed through the changing law of positioning the ball. At the initial stage of loading, the diorite is a hard brittle rock, so no small volume black locating ball is found; with the increasing load, the small and medium volume blue locating ball corresponding to $0.4\sigma_c \sim 0.5\sigma_c$ appears in the middle and upper part of the sample, and new cracks appear in the specimen; with the further increase in load, immediately before a rockburst disaster, $0.98\sigma_c \sim \sigma_c$ orange and red large volume locating balls are distributed along the shear plane. (the peak stress mapping color is different with different unloading rates). The three-dimensional coordinates and stress of acoustic emission positioning events can reflect the catastrophic process of rockburst and can be used as rockburst precursory information.

3.4. Research on the Evolution Law of the b Value. A large number of scholars have found that the value of acoustic emission b can reflect the change law of internal cracks in the process of rock fracture. In this paper, the evolution law of the b value in the catastrophic rockburst process is revealed by analyzing the acoustic emission data of triaxial increasing axial compression and unloading confining pressure. The calculation of the acoustic emission b value was first proposed by Gutenberg and Richter and Ge et al. in the study of seismicity in 1994, which reflects the relationship between earthquake magnitude and frequency [48, 49]. Its expression in Formula (1) shows the following:

$$\lg N = a - bM, \tag{1}$$

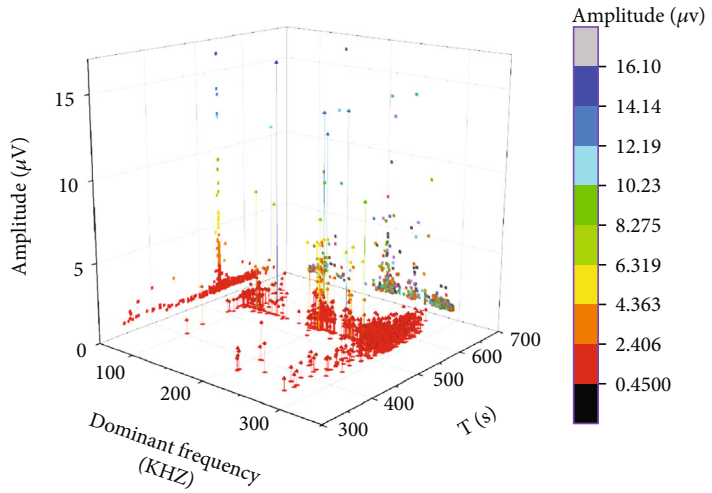

(a) 0.1 MPa/s

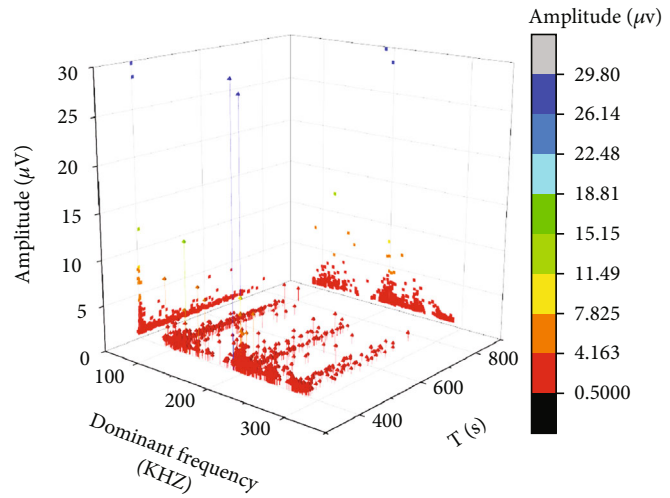

(b) 0.5 MPa/s

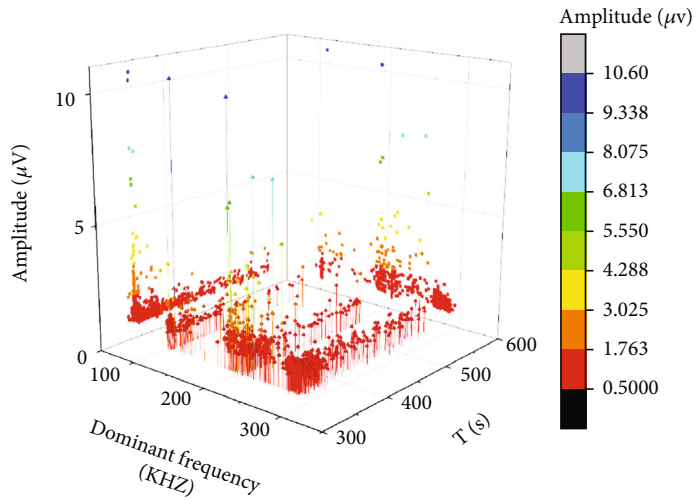

(c) 0.7 MPa/s

Figure 12: Continued.

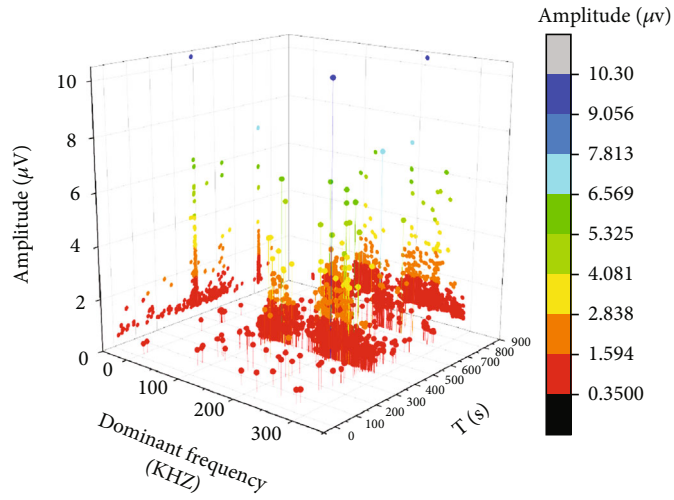

(d) 0.9 MPa/s

Figure 12: Three-dimensional evolution diagram of the main frequency-time-amplitude of the same confining pressure and different unloading rates.

where M is the magnitude of the earthquake, N is the cumulative frequency between magnitude intervals, and a and b are constants.

From the analysis of Figure 10 and Table 1, the maximum decrease rates of b values at 0.1 MPa/s, 0.3 MPa/s, 0.5 MPa/s, and 0.7 MPa/s unloading rates are 0.69, 0.87, 0.94, and 0.51, respectively. The maximum decrease rates are all greater than 0.5, and the crack scale has undergone tremendous changes. It can be seen that immediately prior to rockburst, the value of acoustic emission b falls sharply, the range of low value fluctuates densely, there are large cracks in the rock, and the internal cracks gradually reach the critical range. The b value of acoustic emission can reflect the catastrophic process of rockburst, and the abnormal decrease in the b value of acoustic emission and the fluctuation of the low value can be used as rockburst precursory information.

3.5. Analysis of the Evolution of the Acoustic Emission Spectrum. In this paper, the acoustic emission processing software is compiled based on the MATLAB platform. As shown in Figure 11, the amplitude, main frequency, and time information of the acoustic emission data are extracted by the Fourier transform, and three-dimensional diagrams of the time, frequency, and amplitude of the acoustic emission test are drawn, which directly and efficiently reveal the three characteristics of the time and frequency amplitude of rockburst. In the acoustic emission test, there are few early events in the acoustic emission data. In this paper, the places where the events are concentrated in the rockburst disaster process are analyzed to reveal the evolution law of rockburst precursory information.

As shown in Figures 12(a)–12(d), there are few acoustic emission events in the early stage of loading in the axial compression unloading confining pressure test. After 300 s of acoustic emission tests, the acoustic emission signal increases explosively, immediately before the rockburst. As shown in Figure 12(d), the 272 s ~ 294 s acoustic emission signal appears calm before the explosive growth. After the quiet period, the 363 s low-frequency high amplitude point and high-frequency low amplitude point appear at the same time, and the microcracks in the rock converge and nucleate to form macroscopic failure. Compared with the traditional acoustic emission parameter analysis, waveform data contains a lot of rock fracture information. Fast Fourier transform analysis can be used to extract the main frequency and amplitude information, which can fully capture the precursor information of rockburst. Triaxial acoustic emission probe acquisition information is affected by noise, and waveform data is not easy to collect. At the unloading rate of 0.1 MPa/s, 0.5 MPa/s, 0.7 MPa/s, and 0.9 MPa/s, there are low-frequency and high-amplitude information points before and after the peaks, and large cracks and small cracks converge to nucleate. Therefore, a large amount of low-frequency high amplitude and high-frequency low amplitude acoustic emissions appear at the same time as the rockburst precursory information.

3.6. Analysis of the Evolution Law of Information Entropy. The theory of information entropy is proposed by Shannon's research, which is used to evaluate the uncertainty index of the system and is often used to judge the complexity of equipment fault signals. In this paper, information entropy is introduced to analyze the waveform data of the rock fracture acoustic emission test [50]. The information entropy processing method of acoustic emission test waveform data is proposed, including energy entropy, power spectrum entropy, and singular spectrum entropy.

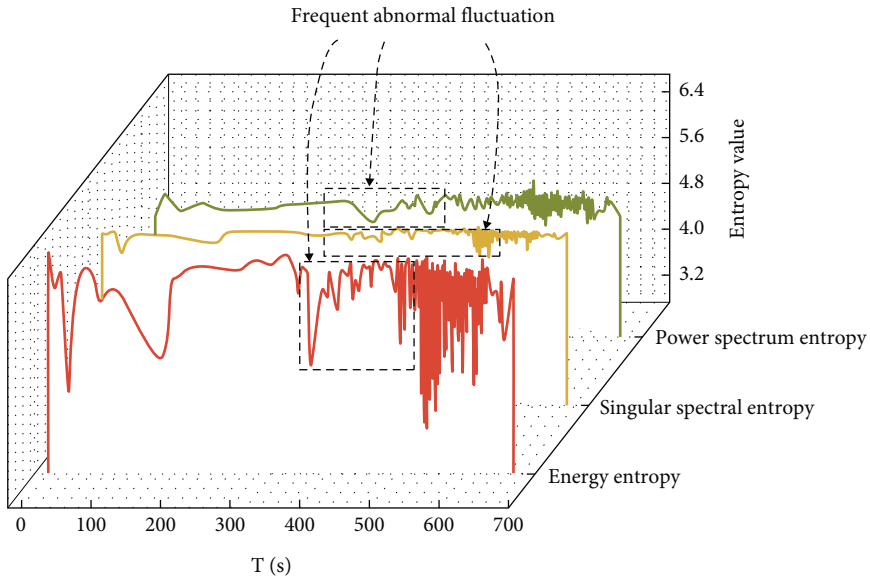

(a) 0.1 MPa/s

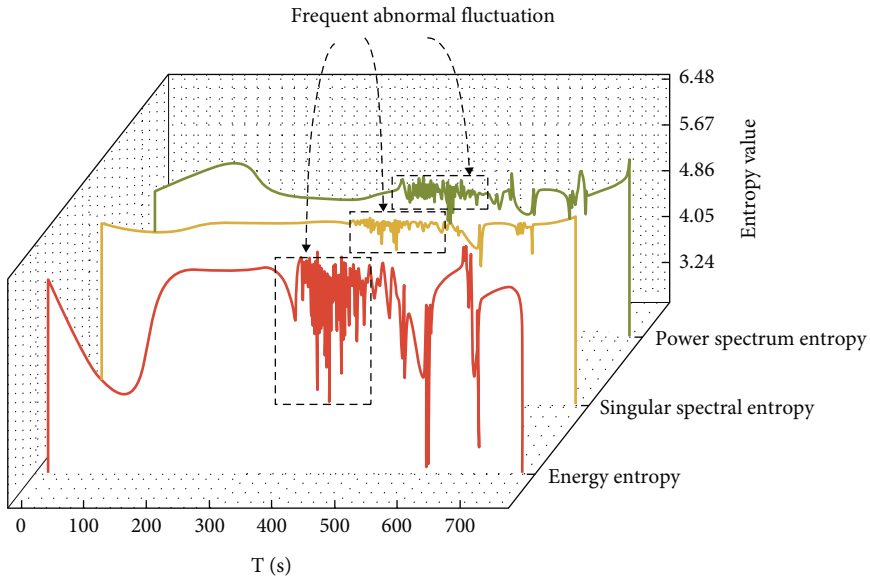

(b) 0.3 MPa/s

Figure 13: Continued.

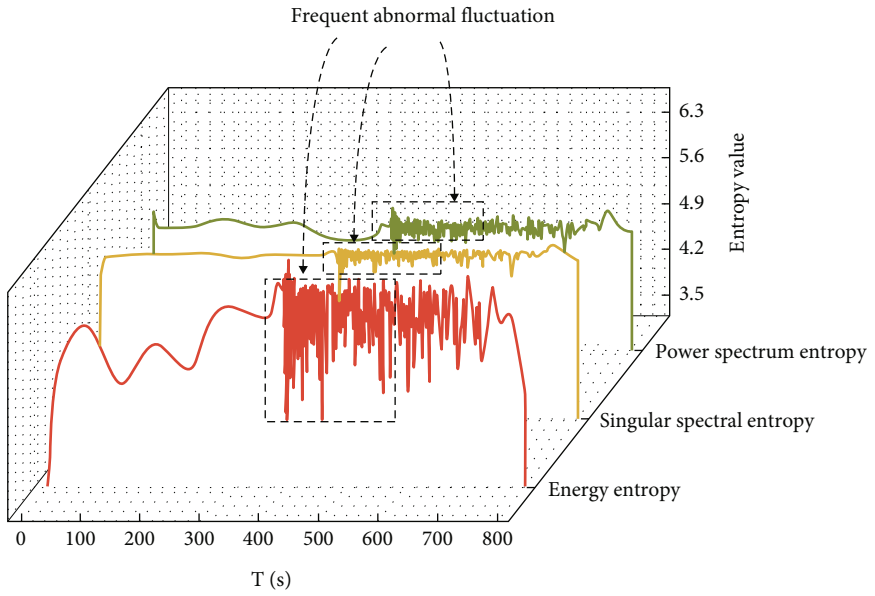

(c) 0.5 MPa/s

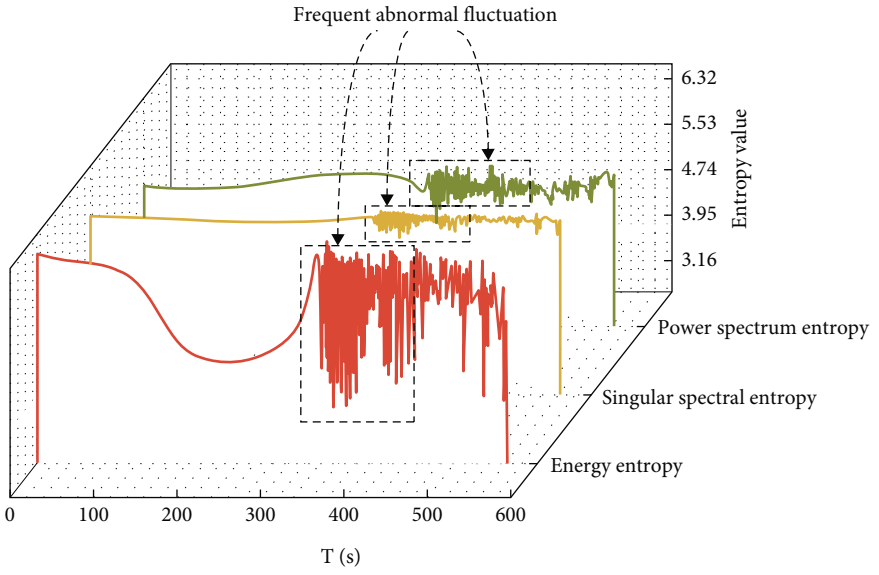

(d) 0.7 MPa/s

Figure 13: Information entropy of the loading process of specimens with the same confining pressure and different unloading rates.

Table 2: Fluctuation schedule of power spectrum entropy, singular spectrum entropy, and energy entropy.

Unloading rate	0.1 MPa/s	0.3 MPa/s	0.5 MPa/s	0.7 MPa/s
Steady sparse fluctuation	0 s ~ 285 s	0 s ~ 321 s	0 s ~ 270 s	0 s ~ 165 s
Frequent abnormal fluctuation	402 s ~ 653 s	367 s ~ 687 s	372 s ~ 776 s	322 s ~ 563 s

Suppose that there are multiple events in a system $x = \{x_1, x_2, \cdots, x_n\}$, and the probability set of each event is $P\{p_1, p_2 \cdots p_n\}$; then, the information entropy $H(x)$ of the whole system is

$$H(x) = E(I(x_i)) = -\sum p_i \log_a p_i, \tag{2}$$

$$I(x_i) = -\log p(x_i) = -\log_a p_i, \tag{3}$$

where $I(x_i)$ represents the amount of information about the event $\sum_{i=1}^{n} p_i = 1$.

(1) The acoustic emission waveform data are collected by the acoustic emission acquisition system, and

the acoustic emission waveform data of six channels are classified. The channels with dense acoustic emission data are selected for data preprocessing, and the sampling time is extracted in batches by using MATLAB software

(2) There are 1024-point data in each waveform, and the sampling time is the same as the sampling time of the spectrum analysis data. The obtained data are imported into MATLAB for batch calculation (functions are defined according to the power spectrum entropy, the singular spectrum entropy, and the energy entropy in MATLAB)

(3) Write the calculated data into the Excel table in batches and save it

(4) The processed Excel data were imported into Origin software to draw the three-dimensional information entropy diagram of the sample loading process. In the acoustic emission test, there are a large number of noise signals in the laboratory, so the reliability of analyzing the acoustic emission test waveform data in the time domain and frequency domain is not sufficiently accurate, and the power spectrum entropy and singular spectrum entropy curves can overcome the influence of noise signals. In this paper, samples with different unloading rates under high confining pressure are analyzed to explore the changing rules of power spectrum entropy, singular spectrum entropy curve, and energy entropy in the catastrophic rockburst process

In Figure 13, the red curve represents the changing law of the energy entropy curve, the orange curve represents the singular entropy curve, and the green curve represents the power spectrum entropy curve. The energy entropy curve, the singular spectrum entropy curve, and the power spectrum entropy curve fluctuate relatively smoothly and sparsely at the initial stage of the confining pressure test. As the load increases immediately before the rockburst, the curves of energy spectrum entropy, singular spectrum entropy, and power spectrum entropy fluctuate abnormally. As shown in Table 2, the above evolution law can reflect the catastrophic rockburst process and can be used as precursory rockburst information.

3.7. Analysis of Test Conclusion and Field Application. Based on the above analysis, the mechanical characteristics of Poisson's ratio and elastic modulus are analyzed. At present, only laboratory tests can be applied to lay a foundation for the theoretical analysis of rockburst precursor information. The relationship between stress and ringing count, energy, acoustic emission positioning information, and b value was established. The laws of ring count (energy) quiet period and surge, burst position information point surge, and b value drop can be applied to the analysis of field monitoring data. Time-frequency-amplitude and information entropy analysis is a method of waveform data analysis. A large amount of waveform data can be obtained by means of ground pressure monitoring in mining process. High-frequency low amplitude and low-frequency high amplitude of time-frequency-amplitude characteristics, energy entropy, power spectrum entropy and singular spectrum entropy abnormal fluctuation can be used as a new method of monitoring data processing to improve the ability of rockburst precursor information identification.

4. Conclusion

(1) Through the triaxial unloading test of loading axial compression and unloading high confining pressure, it is found that Poisson's ratio in the failure process of the rock specimen is in a hook-shape and the elastic modulus is in the shape of a step. Rockburst disasters occur when Poisson's ratio reaches the turning point and the elastic modulus decreases precipitously, which can be considered precursory rockburst information

(2) In the early stage of rockburst, there is a surge in ringing count and energy, and the range of low values of acoustic emission b fluctuates. The above characteristics can reflect the rockburst process and can be considered rockburst precursor information

(3) The acoustic emission waveform data are processed by Fourier transform, and the time-frequency-amplitude characteristics are analyzed. It is found that the characteristics of low-frequency high amplitude and high-frequency low amplitude emissions fluctuate in a large range immediately prior to rockburst, which can be considered as rockburst precursor information

(4) Information entropy is introduced to analyze the power spectrum entropy, singular spectrum entropy, and energy spectrum entropy of the waveform data. The frequent abnormal fluctuations of the curves can be considered as the evolution law of rockburst precursory information

Data Availability

The experimental data of this paper can be obtained from the author.

Conflicts of Interest

The author declares that there is no conflict of interest in the publication of this paper.

Authors' Contributions

The first author is Jian Liu.

Acknowledgments

This work was financially supported by the National Natural Science Foundation of China (nos. 51864023 and 52264019), the Yunnan Major Scientific and Technological Projects of

China (no. 202202AG050014), and the Hubei Key Laboratory for Efficient Utilization and Agglomeration of Metallurgic Mineral Resources Open Foundation of China (no. 2022zy002).

References

[1] H. Farhadian, "A new empirical chart for rockburst analysis in tunnelling: Tunnel rockburst classification (TRC)," *International Journal of Mining Science and Technology*, vol. 31, no. 4, pp. 603–610, 2021.

[2] M. C. He, T. Cheng, Y. F. Qiao, and H. Li, "A review of rockburst: experiments, theories, and simulations," *Journal of Rock Mechanics and Geotechnical Engineering*, vol. 15, no. 5, pp. 1312–1353, 2023.

[3] M. Wu, Y. Ye, Q. Wang, and N. Hu, "Development of rockburst research: a comprehensive review," *Applied Sciences*, vol. 12, no. 3, p. 974, 2022.

[4] J. Wang, D. B. Apel, Y. Y. Pu, R. Hall, C. Wei, and M. Sepehri, "Numerical modeling for rockbursts: a state-of-the-art review," *Journal of Rock Mechanics and Geotechnical Engineering*, vol. 13, no. 2, pp. 457–478, 2021.

[5] J. F. Zhang, F. X. Jiang, J. B. Yang, W. S. Bai, and L. Zhang, "Rockburst mechanism in soft coal seam within deep coal mines," *International Journal of Mining Science and Technology*, vol. 27, no. 3, pp. 551–556, 2017.

[6] P. Jia and W. C. Zhu, "Dynamic-static coupling analysis on rockburst mechanism in jointed rock mass," *Journal of Central South University*, vol. 19, no. 11, pp. 3285–3290, 2012.

[7] Y. Pan, Y. Zhang, and G. M. Yu, "Mechanism and catastrophe theory analysis of circular tunnel rockburst," *Applied Mathematics and Mechanics*, vol. 27, no. 6, pp. 841–852, 2006.

[8] F. Q. Gong, Y. Luo, X. B. Li, X. F. Si, and M. Tao, "Experimental simulation investigation on rockburst induced by spalling failure in deep circular tunnels," *Tunnelling and Underground Space Technology*, vol. 81, pp. 413–427, 2018.

[9] X. C. Hu, G. S. Su, G. Y. Chen et al., "Experiment on rockburst process of borehole and its acoustic emission characteristics," *Rock Mechanics and Rock Engineering*, vol. 52, no. 3, pp. 783–802, 2019.

[10] X. M. Sun, H. C. Xu, M. C. He, and F. Zhang, "Experimental investigation of the occurrence of rockburst in a rock specimen through infrared thermography and acoustic emission," *International Journal of Rock Mechanics and Mining Sciences*, vol. 93, pp. 250–259, 2017.

[11] G. S. Su, Y. J. Shi, X. T. Feng, J. Q. Jiang, J. Zhang, and Q. Jiang, "True-triaxial experimental study of the evolutionary features of the acoustic emissions and sounds of rockburst processes," *Rock Mechanics and Rock Engineering*, vol. 51, no. 2, pp. 375–389, 2018.

[12] J. S. Sun, Q. H. Zhu, and W. B. Lu, "Numerical simulation of rock burst in circular tunnels under unloading conditions," *Journal of China University of Mining and Technology*, vol. 17, no. 4, pp. 552–556, 2007.

[13] W. C. Zhu, Z. H. Li, L. Zhu, and C. A. Tang, "Numerical simulation on rockburst of underground opening triggered by dynamic disturbance," *Tunnelling and Underground Space Technology*, vol. 25, no. 5, pp. 587–599, 2010.

[14] F. J. Yang, H. Zhou, H. B. Xiao, U. A. Muhammad, Y. Zhu, and F. D. Chi, "Numerical simulation method for the process of rockburst," *Engineering Geology*, vol. 306, article 106760, 2022.

[15] A. Manouchehrian and M. Cai, "Numerical modeling of rockburst near fault zones in deep tunnels," *Tunnelling and Underground Space Technology*, vol. 80, pp. 164–180, 2018.

[16] Q. Jiang, X. T. Feng, T. B. Xiang, and G. S. Su, "Rockburst characteristics and numerical simulation based on a new energy index: a case study of a tunnel at 2, 500 m depth," *Bulletin of Engineering Geology and the Environment*, vol. 69, no. 3, pp. 381–388, 2010.

[17] Q. H. Zhu, W. B. Lu, J. S. Sun, Y. Luo, and M. Chen, "Prevention of rockburst by guide holes based on numerical simulations," *Mining Science and Technology (China)*, vol. 19, no. 3, pp. 346–351, 2009.

[18] L. M. Dou, T. J. Chen, S. Y. Gong, H. He, and S. B. Zhang, "Rockburst hazard determination by using computed tomography technology in deep workface," *Safety Science*, vol. 50, no. 4, pp. 736–740, 2012.

[19] I. Y. Rasskazov, D. S. Migunov, P. A. Anikin, A. V. Gladyr', A. A. Tereshkin, and D. O. Zhelnin, "New-generation portable geoacoustic instrument for rockburst hazard assessment," *Journal of Mining Science*, vol. 51, no. 3, pp. 614–623, 2015.

[20] X. T. Feng, J. P. Liu, B. R. Chen, Y. X. Xiao, G. L. Feng, and F. P. Zhang, "Monitoring, warning, and control of rockburst in deep metal mines," *Engineering*, vol. 3, no. 4, pp. 538–545, 2017.

[21] G. F. Liu, Q. Jiang, G. L. Feng, D. F. Chen, B. R. Chen, and Z. N. Zhao, "Microseismicity-based method for the dynamic estimation of the potential rockburst scale during tunnel excavation," *Bulletin of Engineering Geology and the Environment*, vol. 80, no. 5, pp. 3605–3628, 2021.

[22] X. Q. He, C. Zhou, D. Z. Song et al., "Mechanism and monitoring and early warning technology for rockburst in coal mines," *International Journal of Minerals, Metallurgy and Materials*, vol. 28, no. 7, pp. 1097–1111, 2021.

[23] L. R. Sousa, T. Miranda, R. L. Sousa, and J. Tinoco, "The use of data mining techniques in rockburst risk assessment," *Engineering*, vol. 3, no. 4, pp. 552–558, 2017.

[24] Y. Y. Pu, D. B. Apel, V. Liu, and H. Mitri, "Machine learning methods for rockburst prediction-state-of-the-art review," *International Journal of Mining Science and Technology*, vol. 29, no. 4, pp. 565–570, 2019.

[25] S. Y. He, J. X. Lai, Y. J. Zhong et al., "Damage behaviors, prediction methods and prevention methods of rockburst in 13 deep traffic tunnels in China," *Engineering Failure Analysis*, vol. 121, article 105178, 2021.

[26] P. Małkowski and Z. Niedbalski, "A comprehensive geomechanical method for the assessment of rockburst hazards in underground mining," *International Journal of Mining Science and Technology*, vol. 30, no. 3, pp. 345–355, 2020.

[27] M. C. He, F. Q. Ren, and D. Q. Liu, "Rockburst mechanism research and its control," *International Journal of Mining Science and Technology*, vol. 28, no. 5, pp. 829–837, 2018.

[28] J. J. Ren, W. L. Zhang, and J. Ma, "Experimental study on butterfly shape of failure zone and fractal characteristics of rock burst," *Engineering Failure Analysis*, vol. 140, article 106636, 2022.

[29] A. Keneti and B. A. Sainsbury, "Review of published rockburst events and their contributing factors," *Engineering Geology*, vol. 246, pp. 361–373, 2018.

[30] T. H. Ma, C. A. Tang, S. B. Tang et al., "Rockburst mechanism and prediction based on microseismic monitoring," *International Journal of Rock Mechanics and Mining Sciences*, vol. 110, pp. 177–188, 2018.

[31] L. J. Dong, X. B. Li, and K. Peng, "Prediction of rockburst classification using random forest," *Transactions of Nonferrous Metals Society of China*, vol. 23, no. 2, pp. 472–477, 2013.

[32] C. P. Lu, Y. Liu, N. Zhang, T. B. Zhao, and H. Y. Wang, "In-situ and experimental investigations of rockburst precursor and prevention induced by fault slip," *International Journal of Rock Mechanics and Mining Sciences*, vol. 108, pp. 86–95, 2018.

[33] G. F. Wang, S. Y. Gong, L. M. Dou, H. Wang, W. Cai, and A. Y. Cao, "Rockburst characteristics in syncline regions and microseismic precursors based on energy density clouds," *Tunnelling and Underground Space Technology*, vol. 81, pp. 83–93, 2018.

[34] X. X. Liu, Z. Z. Liang, Y. B. Zhang, P. Liang, and B. Z. Tian, "Experimental study on the monitoring of rockburst in tunnels under dry and saturated conditions using AE and infrared monitoring," *Tunnelling and Underground Space Technology*, vol. 82, pp. 517–528, 2018.

[35] W. J. Ding, Z. H. Zhou, J. Liu et al., "Research on the identification of precursor information of limestone rockburst under triaxial unloading conditions," *Geofluids*, vol. 2022, Article ID 3282276, 14 pages, 2022.

[36] Z. Z. Liang, X. X. Liu, Y. B. Zhang, and C. A. Tang, "Analysis of precursors prior to rock burst in granite tunnel using acoustic emission and far infrared monitoring," *Mathematical Problems in Engineering*, vol. 2013, Article ID 214340, 10 pages, 2013.

[37] Y. X. Gong, Z. J. Song, M. C. He, W. L. Gong, and F. Q. Ren, "Precursory waves and eigenfrequencies identified from acoustic emission data based on singular spectrum analysis and laboratory rock-burst experiments," *International Journal of Rock Mechanics and Mining Sciences*, vol. 91, pp. 155–169, 2017.

[38] C. L. Wang, "Experimental investigation on AE precursor information of rockburst," in *Evolution, Monitoring and Predicting Models of Rockburst*, pp. 77–105, Springer, Singapore, 2018.

[39] M. Q. Lin, C. C. Gao, Y. Y. Xia, D. J. Zhang, X. Q. Liu, and X. S. Liang, "Rock burst initiation and precursors in a model specimen based on acoustic emission and infrared monitoring," *Arabian Journal of Geosciences*, vol. 15, no. 4, 2022.

[40] S. Q. He, M. L. Qin, L. M. Qiu, D. Z. Song, and X. F. Zhang, "Early warning of coal dynamic disaster by precursor of AE and EMR "quiet period"," *International Journal of Coal Science & Technology*, vol. 9, no. 1, 2022.

[41] S. B. Zhai, G. S. Su, S. D. Yin, S. Z. Yan, Z. F. Wang, and L. B. Yan, "Fracture evolution during rockburst under true-triaxial loading using acoustic emission monitoring," *Bulletin of Engineering Geology and the Environment*, vol. 79, no. 9, pp. 4957–4974, 2020.

[42] R. X. Xue, Z. Z. Liang, and N. W. Xu, "Rockburst prediction and analysis of activity characteristics within surrounding rock based on microseismic monitoring and numerical simulation," *International Journal of Rock Mechanics and Mining Sciences*, vol. 142, article 104750, 2021.

[43] C. L. Wang, C. Cao, C. F. Li, X. S. Chuai, G. M. Zhao, and H. Lu, "Experimental investigation on synergetic prediction of granite rockburst using rock failure time and acoustic emission energy," *Journal of Central South University*, vol. 29, no. 4, pp. 1262–1273, 2022.

[44] C. L. Wang, Z. Chen, Z. F. Liao et al., "Experimental investigation on predicting precursory changes in entropy for dominant frequency of rockburst," *Journal of Central South University*, vol. 27, no. 10, pp. 2834–2848, 2020.

[45] G. S. Su, W. Gan, S. B. Zhai, and G. F. Zhao, "Acoustic emission precursors of static and dynamic instability for coarse-grained hard rock," *Journal of Central South University*, vol. 27, no. 10, pp. 2883–2898, 2020.

[46] J. X. Chen, O. Chen, F. W. Wang, and Y. P. Wu, "Measurement and analysis of deep geostress distribution in Jinfeng gold mine," *Gold*, vol. 42, no. 1, pp. 42–45, 2021.

[47] S. Q. Li, M. H. Ma, and X. Zhang, "Characteristics of ground stress distribution in Sanshandao gold mining area," *Modern Mining*, vol. 33, no. 1, pp. 202–205, 2017.

[48] B. Gutenberg and C. F. Richter, "Frequency of earthquakes in California," *Bulletin of the Seismological Society of America*, vol. 34, no. 4, pp. 185–188, 1944.

[49] Z. L. Ge, Q. Sun, J. Geng, and H. Zhang, "Thermal effect on b-value of limestone subjected to uniaxial loading," *Arabian Journal of Geosciences*, vol. 14, no. 13, p. 1282, 2021.

[50] D. L. Feng, M. Q. Xiao, Y. X. Liu, H. F. Song, Z. Yang, and Z. W. Hu, "Finite-sensor fault-diagnosis simulation study of gas turbine engine using information entropy and deep belief networks," *Frontiers of Information Technology & Electronic Engineering*, vol. 17, no. 12, pp. 1287–1304, 2016.